Neurochemistry International 126 (2019) 229–238

Contents lists available at ScienceDirect

Neurochemistry International

journal homepage: www.elsevier.com/locate/neuint

Pathological changes in mice with long term cuprizone administration

Taichi Nomura[a,*], Yoshio Bando[b], Hitomi Nakazawa[a], Soshi Kanemoto[a], Shigetaka Yoshida[a]

[a] Department of Functional Anatomy and Neuroscience, Asahikawa Medical University, Midorigaoka-higashi 2-1-1-1, Asahikawa, Hokkaido, 078-8510, Japan
[b] Department of Anatomy, Akita University Graduate School of Medicine, 1-1-1 Hondo, Akita, 010-8543, Japan

ARTICLE INFO

Keywords:
Demyelination
Cuprizone
Parvalbumin
Striatum
Multiple sclerosis

ABSTRACT

Multiple sclerosis (MS) is an inflammatory demyelinating disease of the central nervous system (CNS). In MS, a long disease duration is known to be a strong risk factor for converting the clinical course of the disease from relapse remitting MS to secondary progressing MS. There is a hypothesis that long sustained demyelination may exhaust neurons, however, pathological changes induced in neurons following demyelination remain unknown. Cuprizone administration can induce and sustain demyelination in the mouse CNS. We examined pathological changes in mice following long sustained demyelination caused by up to 34-week cuprizone administration. Twelve-week cuprizone administration induced severe demyelination in the cerebral cortex, corpus callosum and deep cerebellar nuclei. Demyelination persisted up to 34 weeks, as shown by myelin basic protein immunohistochemistry. In contrast, cuprizone administration developed demyelination in the striatum by week 34. In these demyelinated regions, no neuronal loss was observed. However, in the striatum and deep cerebellar nuclei, cuprizone-induced demyelination changed the intracellular distribution of parvalbumin (PV). Furthermore, in the striatum, there was an increase in PV in the demyelinated axons and most PV immunoreactivity did not co-localize with SMI32 immunoreactivity in mice with 34-week cuprizone administration. Further, mice with 34-week cuprizone administration showed motor coordination dysfunction in the balance beam test. However, 12-week withdrawal from the cuprizone diet induced remyelination in the regions and motor coordination dysfunction recovered. These results indicate that 34-week cuprizone administration induces and sustains demyelination and results in reversible motor coordination dysfunction. The change of intracellular PV distribution suggests that PV may protect demyelinated axons by Ca^{2+} buffering. This model may be useful to investigate pathological and behavioral changes following demyelination in the CNS.

1. Introduction

Multiple sclerosis (MS) is an inflammatory demyelinating disease of the central nervous system (CNS) that results in many neurological disabilities (Reich et al., 2018). Patients with MS often start clinical courses treating the inflammatory disease, but within 20 years of diagnosis, most of them convert their clinical courses to treat the progressive neurodegenerative disease independent of inflammation (Correale et al., 2017; Kipp et al., 2017; Larochelle et al., 2016; Vukusic and Confavreux, 2003). Although many efficient disease-modifying therapies ameliorate inflammatory attacks in MS, drugs to suppress neurodegeneration following demyelination remain elusive (Correale et al., 2017; Kipp et al., 2017; Kutzelnigg et al., 2005; Larochelle et al., 2016). Therefore, uncovering the mechanisms underlying the induction of neurodegeneration following demyelination in MS is of great importance. Since longer disease duration is a powerful risk factor for neurodegeneration (Calabrese, 2013; Kutzelnigg et al., 2005; Larochelle et al., 2016; Vukusic and Confavreux, 2003), one hypothesis is that accumulation of damage exhausts CNS trophic factors and compensatory mechanisms arise (Calabrese, 2013; Larochelle et al., 2016). However, the pathological changes induced in neurons following sustained demyelination remain unknown.

Cuprizone-induced demyelination is often used as a model of MS in mice (Kipp et al., 2017; Matsushima and Morell, 2001; Groebe et al., 2009; Gudi et al., 2014). In the cuprizone model, demyelination is induced in the corpus callosum, cerebral cortex, striatum and cerebellum (Kipp et al., 2017; Matsushima and Morell, 2001; Groebe et al., 2009; Gudi et al., 2014; Skripuletz et al., 2008; Pott et al., 2009). In addition, demyelination persists during continuous cuprizone feeding (Matsushima and Morell, 2001; Gudi et al., 2014; Skripuletz et al., 2008). Furthermore, withdrawal of cuprizone administration leads to remyelination (Kipp et al., 2017; Matsushima and Morell, 2001; Gudi et al., 2014; Skripuletz et al., 2008). For these reasons, cuprizone-induced demyelination is well used to understand the pathological

* Corresponding author.
E-mail address: t-nomura@asahikawa-med.ac.jp (T. Nomura).

https://doi.org/10.1016/j.neuint.2019.03.018
Received 25 January 2019; Received in revised form 8 March 2019; Accepted 26 March 2019
Available online 30 March 2019
0197-0186/

Abbreviations

CNS	central nervous system
MS	multiple sclerosis
PV	parvalbumin
MBP	myelin basic protein

mechanisms of demyelination and remyelination in the CNS. However, how cuprizone administration of longer than 12 weeks affects neurons in the CNS is unknown.

Here mice were fed a cuprizone diet for up to 34 weeks to examine the pathological and behavioral changes following sustained demyelination in the CNS.

2. Materials and methods

2.1. Animals

All experimental protocols were carried out in accordance with the "Principles of laboratory animal care" guidelines provided by the National Institutes of Health, USA, regarding the care and use of animals for experimental procedures. All experimental protocols were approved by the Institutional Animal Care and Use Committee of Asahikawa Medical University. All efforts were made to minimize animal suffering, to reduce the number of animals used, and to utilize alternatives to *in vivo* techniques, if possible. Female C57BL/6 mice were obtained from the Center for Advanced Research and Education, Asahikawa Medical University Animal Laboratory for Medical Research, (Hokkaido, Japan). Mouse chow containing 0.2% cuprizone (bis-cyclohexanone oxaldihydrazone; Sigma, St. Louis, MO, USA) was custom-synthesized (Oriental Yeast Co. LTD, Chiba, Japan). To induce demyelination in 6-week-old female C57BL/6 mice (n = 12–14 animals per experimental group), animals were administered a normal diet or a 0.2% cuprizone containing diet for 4–34 weeks, as previously described (Bando et al., 2015; Nomura et al., 2017; Tanaka et al., 2013).

2.2. Histochemistry & immunohistochemistry

Mice (n = 5–8 animals per experimental group) were deeply anesthetized using medetomidine (0.3 mg/kg, Nihon Zenyaku Kogyo, Fukushima, Japan), midazolam (4.0 mg/kg, Sando, Tokyo, Japan), and butorphanol (5.0 mg/kg, Meiji Seika Pharma, Tokyo, Japan), then perfused with phosphate buffered saline solution (PBS) followed by 4% paraformaldehyde (PFA) in 0.1 M phosphate buffer (PB, pH 7.4). Mouse brains were removed and immersed in the same fixative solution overnight at 4 °C. Mouse brains were cryoprotected using 0.1 M PB containing 30% sucrose for 2 days at 4 °C and then frozen in Optimal Cutting Temperature compound. Frozen 10-μm-thick sections were cut from their tissue blocks using a cryostat. To assess the extent of demyelination, luxol fast blue (LFB) staining was performed. Sections were rehydrated in 95% ethanol and immersed in the 0.01% LFB solution overnight at 55 °C. Sections were then differentiated using a 0.05% lithium carbonate and 70% ethanol solution. For immunohistochemistry, rat monoclonal anti-myelin basic protein (MBP) antibody (1:500, Abcam, Cambridge, UK), anti-Iba-1 antibody (1:1000, Wako, Osaka, Japan), mouse anti-NeuN antibody (1:500, Millipore, Frankfurt, Germany), rabbit polyclonal anti-parvalbumin antibody (1:3000, Abcam, Cambridge, UK), mouse anti-SMI32 antibody (1:1000, BioLegend, San Diego, CA, USA), mouse anti-amyloid precursor protein antibody (1:1000, Millipore, Frankfurt, Germany). Immunofluorescence staining was performed as previously reported (Bando et al., 2015; Nomura et al. 2013, 2017). In brief, after drying, the sections were incubated with a solution containing 5% bovine serum albumin and 0.3% Triton-X for 60 min. Then those sections were incubated with primary antibodies at 4 °C overnight. Sections were then incubated with either Alexa-488-conjugated or Alexa-594-conjugated secondary antibodies (1:500–1000, Molecular probes, Eugene, OR, USA) at room temperature for 1 h followed by nuclear staining with 4′,6-diamidino-2-phenylindole (DAPI, Sigma, St. Louis, MO, USA). Sections were then imaged by a confocal laser scanning microscope (Olympus, Tokyo, Japan). For immunohistochemistry with 3,3′-Diaminobenzidine, tetrahydrochloridedetection, after incubating with the primary antibody, sections were immersed in 1.5% H_2O_2 in methanol for 15 min to block endogenous peroxidase activity. Then using a VECTASTAIN ABC kit (Funakoshi, Tokyo, Japan) and 0.02% DAB solution in 50 mM Tris-HCl (pH 7.4) buffer. By analysis software (Olympus, Tokyo, Japan), we counted the number of neurons that stained positive with anti-NeuN antibodies.

2.3. Transmission electron microscopy (TEM)

Animals (n = 3 animals per experimental group) were perfused with 2% glutaraldehyde (GA) and 4% PFA in 0.1 M PB. The brains were removed and 100-μm-thick sections were cut by a DSK MICROSLICER (DTK-3000). Then, the sections were fixed with 1% OsO_4 and embedded in Epon, as previously described (Bando et al., 2015; Nomura et al., 2013). Ultrathin sections were cut and stained with 4% uranium acetate and lead citrate and observed under a transmission electron microscope (H-7650, Hitachi, Japan).

2.4. Pre-embedding immunoelectron microscopy

Animals (n = 3 animals per experimental group) were perfused with 0.5% GA and 4% PFA in 0.1 M PB. The brains were removed and 50-μm sections were cut by a DSK MICROSLICER (DTK-3000). The sections were blocked with a solution containing 5% bovine serum albumin in PBS for 1 h. Then the sections were incubated with a rabbit anti-parvalbumin antibody (1:3000, Abcam, Cambridge, UK) overnight. Using a VECTASTAIN ABC kit as described above, a DAB reaction was performed. After fixation with 2% GA and 4% PFA, sections were further fixed with 1% OsO_4 and embedded in Epon.

2.5. In situ hybridization

Parvalbumin (PV) probes were made by the following primers: PV sense primer 5′-CGCTGAGGACATCAAGAAGG-3'; PV anti-sense primer 5′-GCCACTTTTGTCTTTGTCCA-3'. *In situ* hybridization was performed by digoxigenin (DIG; Roche Molecular Biochemicals, Mannheim, Germany) labeled cRNA probes of parvalbumin in the method previously described (Chen et al., 1998; Terayama et al., 2004; Yoshida et al., 1994). Briefly, frozen 10-μm sections were treated with 10 mg/ml protenase K containing buffer. Following fixation with 4% PFA, sections were incubated in acetic anhydride in 0.1 M triethanolamine. Then, the sections were dehydrated and defatted with ethanol and chloroform. Prehybridization was performed with a hybridization buffer (50% deionized formamide, 10% dextran sulfate, 0.2% sarcosyl, 0.5 mg/ml of yeast tRNA, 0.2 mg/ml of denatured salmon sperm DNA and 1 × Denhardt's solution) for 1 h at 55 °C. Then, sections were incubated with DIG-labeled cRNA probes of parvalbumin in a hybridization buffer overnight at 55 °C. Following washing with 50% formamide, 2xSSC, the sections were treated with an Rnase A buffer to remove excess probes. After incubation with a 1.5% Roche blocking reagent in 100 mM malenic acid and 150 mM NaCl, the sections were reacted with 1:500 of an alkaline phosphatase-anti-digoxygenin antibody (Roche Molecular Biochemicals, Mannheim, Germany). Parvalbumin immunoreactivity was visualized with 3.75 μl/ml of 5-bromo-4-chloro-3-indolyl phosphate (BCIP, Roche Molecular Biochemicals, Mannheim, Germany) and 5 μl/ml of nitroblue tetrazolium (NBT, Roche Molecular Biochemicals, Mannheim, Germany) in 100 mM Tris-HCl, 100 mM NaCl and 50 mM MgCl2, pH 9.5.

2.6. Balance beam test

To assess motor coordination disorders, a balance beam test was performed as described before (Chort et al., 2013; Luong et al., 2011). All balance beams were made of wood. Mice (n = 12–14 animals per experimental group) crossed the 80 cm long, 10 mm diameter beam, 95 cm above cushions to protect the mice if they fell. A desk lamp was set on the start platform to serve as an aversive stimulus. At the end of the beam, a black box was placed containing nesting materials from the home cages of the mice. All mice crossed the beam in three consecutive days. The first two days were for training, and the last day was the test. On the test day, we captured mice crossing the beam twice with a video camera and we counted the number of foot slips and the number of time the mice dropped from the beam in a blind manner and calculated the average foot slips for each mouse and the ratio of dropping mice from the beam.

2.7. Data analysis

For semi-quantitative analysis, intensities of MBP immunoreactivity were measured using ImageJ software. Iba1 immunoreactive structures that were located completely around the DAPI-stained nuclei were counted as microglia. These analyses were conducted by an investigator blinded to the treatment groups to omit the bias.

2.8. Statistics

Welch's t-test was used to compare differences between mean values for two groups. When we compared differences of mean values among three or more groups, we used a one-way ANOVA, followed by a Tukey-Kramer test. To compare differences of rate values, we used Fisher's exact test. Differences were deemed statistically significant if they exceeded the 95% confidence interval ($p < 0.05$).

3. Results

3.1. Cuprizone induced demyelination in the CNS

Mice were fed chow supplemented with 0.2% cuprizone for up to 34 weeks to induce and sustain demyelination. First, we examined the time course of cuprizone-induced demyelination by performing myelin basic protein (MBP) immunohistochemistry (Fig. 1). In the control mice, MBP immunoreactivity was evenly detected in the corpus callosum, the cerebral cortex, striatum and deep cerebellar nuclei (Fig. 1a,f and k). Twelve-week cuprizone administration decreased MBP immunoreactivity in the corpus callosum, cerebral cortex and deep cerebellar nuclei (Fig. 1b and g). In these regions, the decrease in MBP immunoreactivity was sustained until 34 weeks of cuprizone administration (Fig. 1c,d,m and n). In contrast, the decrease in MBP immunoreactivity in the striatum did not reach its peak until 12 weeks and at 34 weeks the greatest decrease in immunoreactivity was observed (Fig. 1g,h and i). The relative intensity of MBP immunoreactivity was significantly reduced by cuprizone administration compared with control mice in the cerebral cortex (control: 100.00 ± 13.82%, cuprizone 12w: 33.14 ± 4.77%, cuprizone 22w: 36.81 ± 2.87%, cuprizone 34w: 22.25 ± 4.73%) (Fig. 1e), striatum (control: 100.00 ± 11.49%,

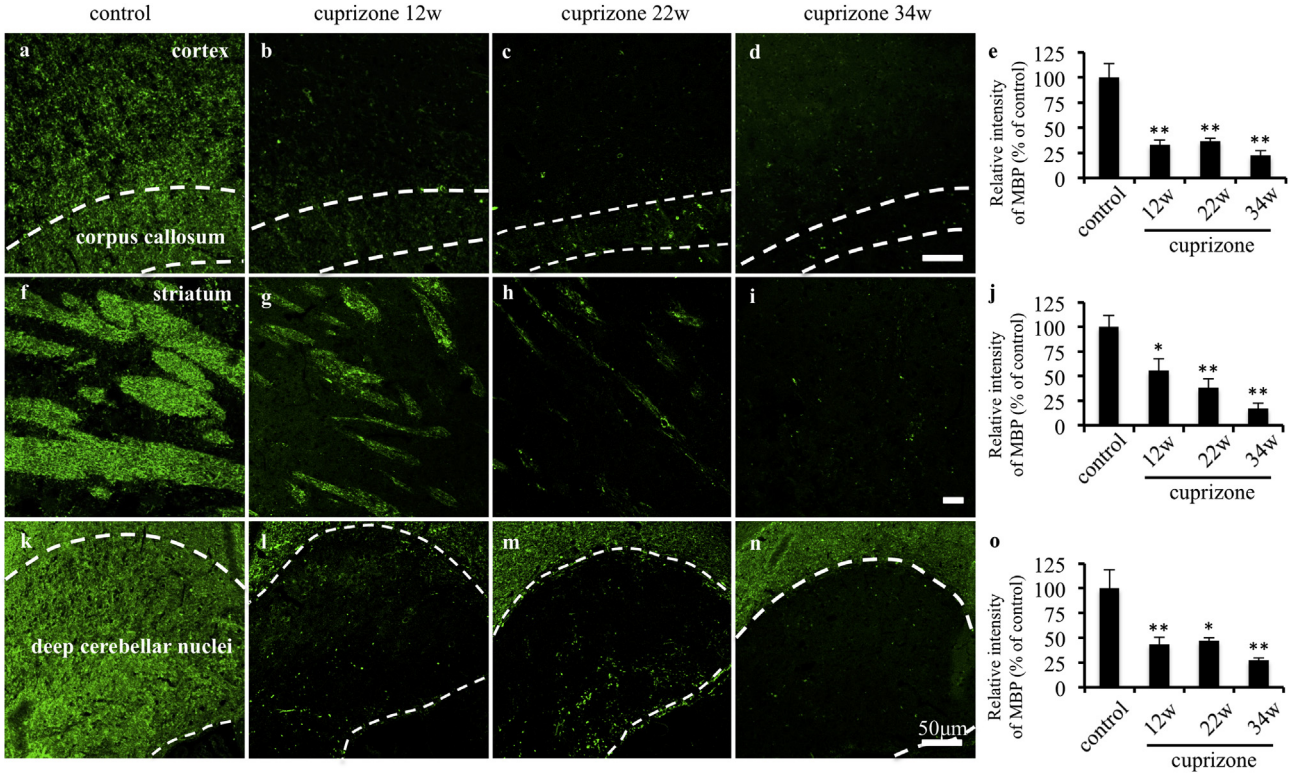

Fig. 1. Cuprizone administration induced demyelination shown by MBP immunohistochemistry.
Representative images of MBP immunohistochemistry in the corpus callosum and cerebral cortex (a–d), striatum (f–i) and deep cerebellar cortex (DCN) (k–n) in mice with control or 12–34-week cuprizone diet are shown. In the corpus callosum and cerebral cortex, while strong MBP immunoreactivity was detected in control mice (a), in mice with 12-week cuprizone administration, MBP immunoreactivity decreased (b). The decrease in MBP immunoreactivity was sustained by 34-week cuprizone administration (c,d). In the deep cerebellar nuclei, while strong MBP immunoreactivity was detected in control mice (k), in mice with 12-week cuprizone administration, MBP immunoreactivity decreased (l). The decrease in MBP immunoreactivity was sustained by 34-week cuprizone administration (m,n). In contrast, in the striatum, MBP immunoreactivity was decreased gradually by cuprizone administration (f–i). Scale bar = 50 μm. Semi-quantitative assessments of the intensity of MBP immunoreactivity in the cerebral cortex (e), striatum (j) and deep cerebellar nuclei (o) are shown in the graphs. Data were obtained from such images from 5 animals in each group (mean ± SEM; **P < 0.01, *P < 0.05 relative to control, one-way ANOVA with Tukey-Kramer post hoc test).

cuprizone 12w: 55.63 ± 12.14%, cuprizone 22w: 38.34 ± 8.69%, cuprizone 34w: 17.13 ± 5.32%) (Fig. 1j) and deep cerebellar nuclei (control: 100.00 ± 18.73%, cuprizone 12w: 43.40 ± 7.18%, cuprizone 22w: 46.91 ± 3.32%, cuprizone 34w: 27.26 ± 2.33%) (Fig. 1o). In the striatum, though not significant, longer cuprizone administration tended to reduce the relative intensity of MBP immunoreactivity (Fig. 1j). On the other hand, MBP immunoreactivity in the brainstem and spinal cord were preserved even in 34-week cuprizone administrated mice (Appendix: Supplementary Figs. S1a–d). Although luxol fast blue (LFB) staining was not sensitive enough to detect myelination in the cerebral cortex (Appendix: Supplementary Fig. S2a), the progression of cuprizone-induced demyelination in the corpus callosum, deep cerebellar nuclei and striatum shown by LFB staining were consistent with the results of MBP immunohistochemistry (Appendix: Supplementary Fig. S2).

Microglia are known to promote cuprizone-induced demyelination in the corpus callosum (Gudi et al., 2014; McMahon et al., 2001; Pasquini et al., 2007). Therefore, we examined whether microglia are activated in the deep cerebellar nuclei and striatum. Four-week cuprizone administration significantly increased the number of microglia in the deep cerebellar nuclei (control: 16.4 ± 1.5/field, cuprizone 4w: 160.4 ± 13.0/field) (Appendix: Supplementary Fig.S3a,b and f), and in the white matter of the striatum (control: 22.4 ± 3.9/field, cuprizone 4w: 61.2 ± 7.1/field) (Appendix: Supplementary Fig.S4a,b and f). The number of microglia significantly decreased thereafter in the cerebellum (cuprizone 12w: 66.6 ± 9.2/field, cuprizone 22w: 42.8 ± 6.2/field, cuprizone 34w: 33.0 ± 3.2/field) (Appendix: Supplementary Figs. S3c–f) while the number of microglia sustained thereafter in the striatum (cuprizone 12w: 54.4 ± 8.7/field, cuprizone 22w: 63.4 ± 3.0/field, cuprizone 34w: 45.8 ± 11.2/field) (Appendix: Supplementary Figs. S4c–f).

3.2. No neuronal loss was observed by cuprizone administration

Next, we examined whether sustained demyelination resulted in neuronal loss. Brain sections of control and 34-week cuprizone-fed mice were immunostained with anti-NeuN antibody. We counted the number of NeuN-positive neurons in the cerebral cortex, deep cerebellar nuclei and striatum. (Fig. 2). The numbers of NeuN-positive cells in control mice (cerebral cortex: 608.9 ± 30.2/field, deep cerebellar nuclei: 192.5 ± 9.3/field, striatum: 251.3 ± 10. 9/field) were not significantly different from those in 34-week cuprizone-fed mice (cerebral cortex: 633.2 ± 23.4/field, deep cerebellar nuclei: 205.4 ± 10.5/field, striatum: 280.1 ± 11.8/field) (Fig. 2g–i). However, the deep cerebellar nuclei area and the white matter areas in the striatum in 34-week cuprizone-fed mice were smaller than those in control mice possibly due to demyelination.

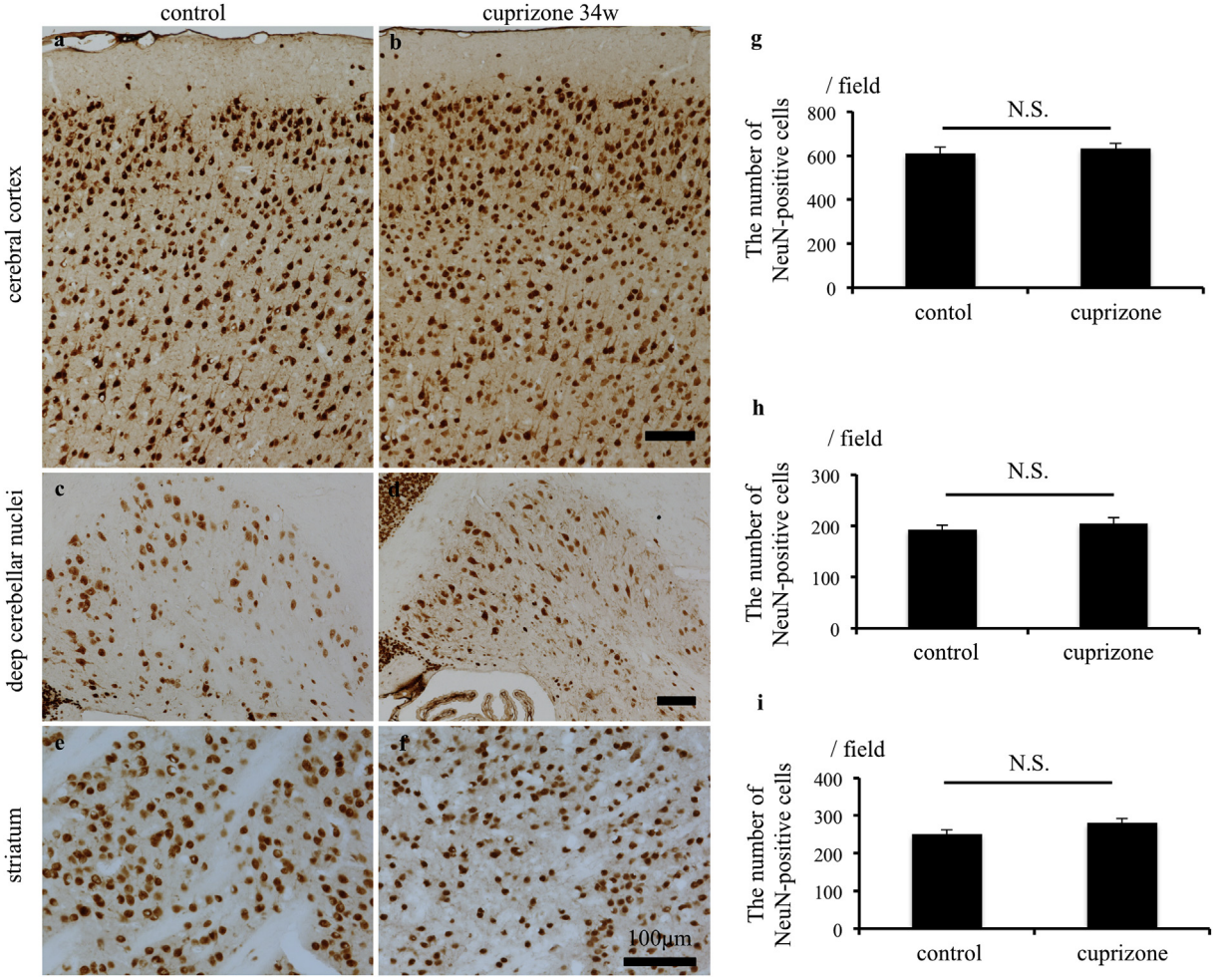

Fig. 2. No neuronal loss was induced by cuprizone administration.
Representative images in mice with or without cuprizone administration in the cerebral cortex (a,b), deep cerebellar nuclei (c,d) and striatum (e,f) by NeuN immunostaining. Scale bar = 100 μm. Quantitative analysis was performed. The number of NeuN positive cells per field in the cerebral cortex (g), deep cerebellar nuclei (h) and striatum (i) are shown in the graphs. Data were obtained from 5 animals in each group (mean ± SEM; **P < 0.05, Welch's *t*-test).

3.3. Cuprizone-induced demyelination changed the intracellular distribution of parvalbumin in the deep cerebellar nuclei and striatum

The cerebral cortex, deep cerebellar nuclei and striatum contain many parvalbumin (PV) neurons. PV is a member of the EF-hand family of calcium-binding proteins and is expressed in subpopulations of neurons (Baimbridge et al., 1992; Celio and Heizmann, 1981; Krieger et al., 1994). Previous reports showed that PV-positive neurons were impaired in the brains of MS patients and in experimental autoimmune encephalomyelitis, another mouse model of MS, (Clements et al., 2008; Dutta et al., 2006; Falco et al., 2014). Therefore, we examined changes in PV-positive structures. In the cerebral cortex, relatively small PV-positive neuronal somata were observed in control mice (Appendix: Supplementary Fig. S5a). The PV staining pattern in the cerebral cortex was not affected by 34-week cuprizone administration (Appendix: Supplementary Fig. S5b). PV immunoreactivity was strongly detected in relatively large neuronal somata and in the neuropil of control deep cerebellar nuclei (Fig. 3a). At 12-week cuprizone administration, PV immunoreactivity in the neuronal somata disappeared and unidentified structures were rather evenly stained (Fig. 3b). This PV staining pattern in the deep cerebellar nuclei persisted with 34-week cuprizone administration (Fig. 3c). In the striatum, relatively small PV-positive neuronal somata and axons in white matter areas were observed in control mice (Fig. 3d). Twelve-week cuprizone administration decreased PV staining in white matter areas without changing PV-positive cell bodies (Fig. 3e). However, at 34-week cuprizone administration, PV staining in white matter areas further decreased but many discrete PV-positive axons appeared, although PV-positive neuronal somata were still observed (Fig. 3f arrowheads).

The next question we had is whether or not PV is still expressed by neuronal cells after cuprizone challenge. We analyzed the expression of PV-mRNA by *in situ* hybridization. In control mice, we detected PV-mRNA positive neurons in the cerebral cortex, deep cerebellar nuclei and striatum (Fig. 4a,c and e). These PV-mRNA signals were not affected by 34-week cuprizone administration (Fig. 4b,d and f). The results of immunohistochemistry and *in situ* hybridization of PV suggest that the intracellular distribution of PV in the deep cerebellar nuclei and striatum was changed by cuprizone-induced demyelination.

3.4. PV is localized in demyelinated axons but not in damaged axons

In the striatum, the distribution of PV drastically changed after 34-week cuprizone administration. While only dot-like PV immunoreactivity was observed in control mice (Fig. 5a), much fiber-like PV immunoreactivity was detected in mice following 34-week cuprizone administration (Fig. 5b). Pre-embedding immunoelectron microscopy revealed that there were few PV-positive axons in control mice (Fig. 5c), PV-positive demyelinated axons were observed in mice with 34-week cuprizone administration (Fig. 5d). Moreover, TEM analysis revealed that many PV-negative myelinated axons were observed in the striatum in control mice (Fig. 5e). After 34-week cuprizone administration, many demyelinated axons were detected (Fig. 5f). Consistent with these results, amyloid precursor protein (APP), a marker of axonal degeneration, was negative in the striatum in both control mice and in mice with 34-week cuprizone administration (Appendix: Supplementary Fig. S6). However, many SMI32-positive fibers (another marker of axonal damage) were observed in mice with 34-week cuprizone administration (Fig. 5h). Most PV-positive fiber-like immunoreactivity did not overlap with SMI32 immunoreactivity in the striatum in mice with 34-week cuprizone administration (Fig. 5l).

3.5. Long term cuprizone administration induced motor coordination disorder

The cerebral cortex, deep cerebellar nuclei and striatum play pivotal roles in coordinated movement. Thus, we used a balance beam test to examine whether coordinated movement was impaired by cuprizone-induced demyelination. In control mice and mice with 4 or 12-week cuprizone administration, there were few foot slips across the beam (control: 0.93 ± 0.20, cuprizone 4w: 0.96 ± 0.27, cuprizone 12w:

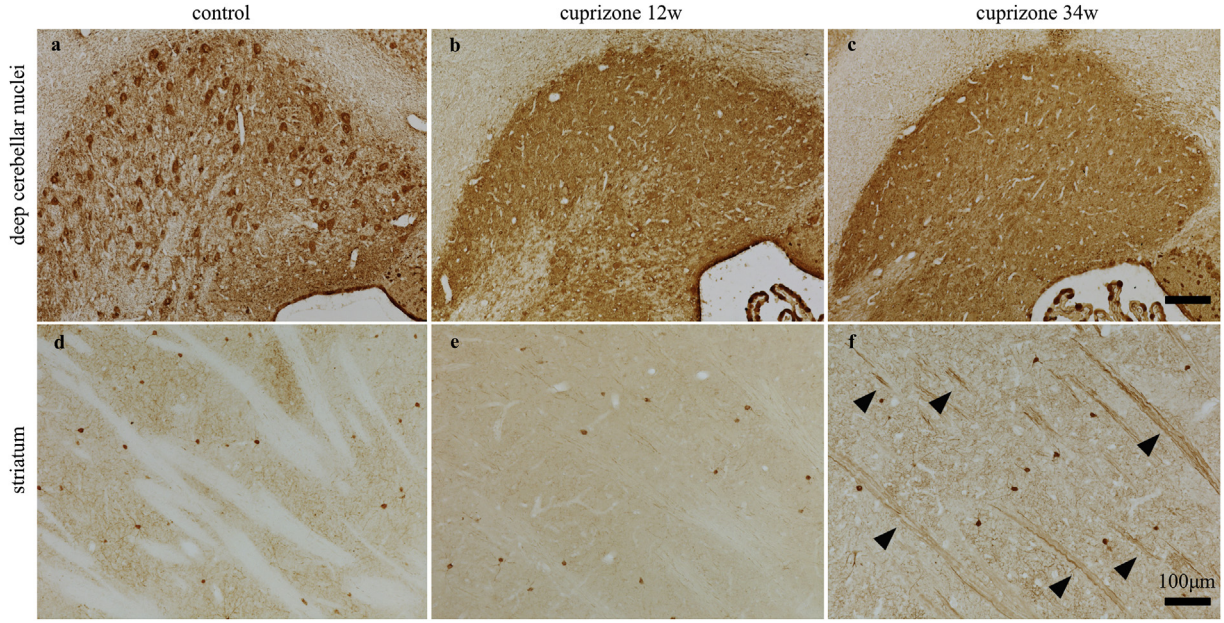

Fig. 3. Cuprizone administration changed the PV immunostaining pattern in the deep cerebellar nuclei and striatum.
Representative images in control and 12 or 34-week cuprizone administered mice in the deep cerebellar nuclei (a–c) and striatum (d–f) stained with PV are shown. In the deep cerebellar nuclei, relatively large PV-positive neuronal somata were observed in control mice. (a) By 12 or 34-week cuprizone administration, PV-immunoreactivity was stained evenly in the deep cerebellar nuclei (b,c). In the striatum, relatively small PV-positive neuronal somata and white matter areas were observed in control mice (d). In mice with 12-week cuprizone administration, although the PV staining pattern was not changed, white matter areas were decreased (e). In mice with 34-week cuprizone administration, white matter areas were further decreased and PV-positive fiber-like immunoreactivity (arrowheads) was observed (f). Scale bar = 100 μm.

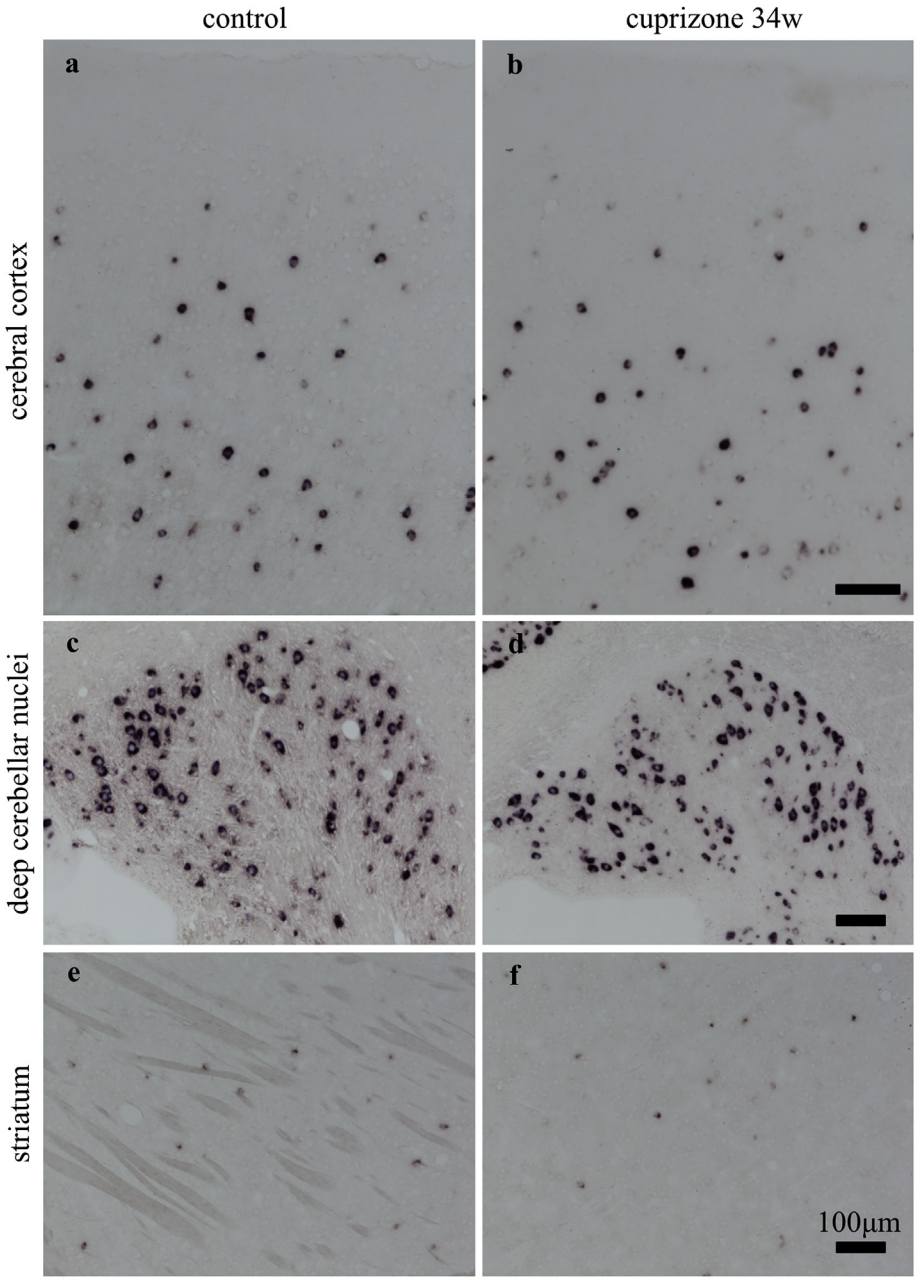

Fig.4 Nomura et al.

Fig. 4. The PV mRNA expression pattern revealed by *in situ* hybridization was not affected in the cerebral cortex, deep cerebellar nuclei or striatum by 34-week cuprizone administration.
Representative images of PV *in situ* hybridization in the cerebral cortex (a,b), deep cerebellar nuclei (c,d) and striatum (e,f) in mice with control or 34-week cuprizone diet are shown. In the cerebral cortex, relatively small PV-positive neuronal nuclei were observed (a) and 34-week cuprizone administration did not affect the PV staining pattern (b). In the deep cerebellar nuclei, relatively large PV-positive neuronal nuclei were observed in control mice (c). In mice with 34-week cuprizone administration, although the area of deep cerebellar nuclei was decreased due to demyelination, relatively large PV-positive neuronal nuclei were still observed (d). In the striatum, relatively small PV-positive nuclei and white matter areas were observed in control mice (e). In mice with 34-week cuprizone administration, although white matter areas were decreased, the PV staining pattern was not affected (f). Scale bar = 100 μm.

1.13 ± 0.25) and no mice fell off the beam (Fig. 6). However, mice with 22 and 34-week cuprizone administration showed significantly more foot slips (cuprizone 22w: 12.50 ± 1.98, cuprizone 34w: 11.40 ± 2.13) crossing the beam compared to control mice and, though not significant, an increased number of cuprizone-fed mice dropped from the beam (cuprizone 22w: 14.29%, cuprizone 34w: 28.57%) (Fig. 6).

3.6. Withdrawal from cuprizone chow induced remyelination and the recovery of motor coordination

It is well known that cuprizone-induced demyelination is reversed by withdrawal of cuprizone chow (Kipp et al., 2017; Matsushima and Morell, 2001; Gudi et al., 2014; Skripuletz et al., 2008). This recovery has been reported in mice fed cuprizone for up to 12 weeks. To examine whether remyelination was also induced by withdrawal of cuprizone chow after a longer period of cuprizone feeding, we gave mice a normal diet for up to 12 weeks following 22 weeks of cuprizone feeding. In control mice, MBP was rich in the cerebral cortex, striatum and deep cerebellar nuclei (Fig. 7a,e and i). MBP immunoreactivity decreased in these regions following 22-week cuprizone administration (Fig. 7b,f and j). MBP immunoreactivity in the cerebral cortex, striatum and deep cerebellar nuclei was partially but significantly recovered by 12-week administration of a normal diet following 22-week cuprizone administration (Fig. 7c,g and k). The relative intensity of MBP immunoreactivity was significantly reduced by 22-week cuprizone administration compared with control mice, but significantly recovered by 12-week administration of a normal diet following 22-week cuprizone administration in the cerebral cortex (control: 100.00 ± 11.21%, cuprizone 22w: 31.74 ± 3.36%, cuprizone 22w Reverse 12w: 79.92 ± 9.68%) (Fig. 7d), striatum (control: 100.00 ± 9.45%, cuprizone 22w: 39.28 ± 6.77%, cuprizone 22w Reverse 12w:

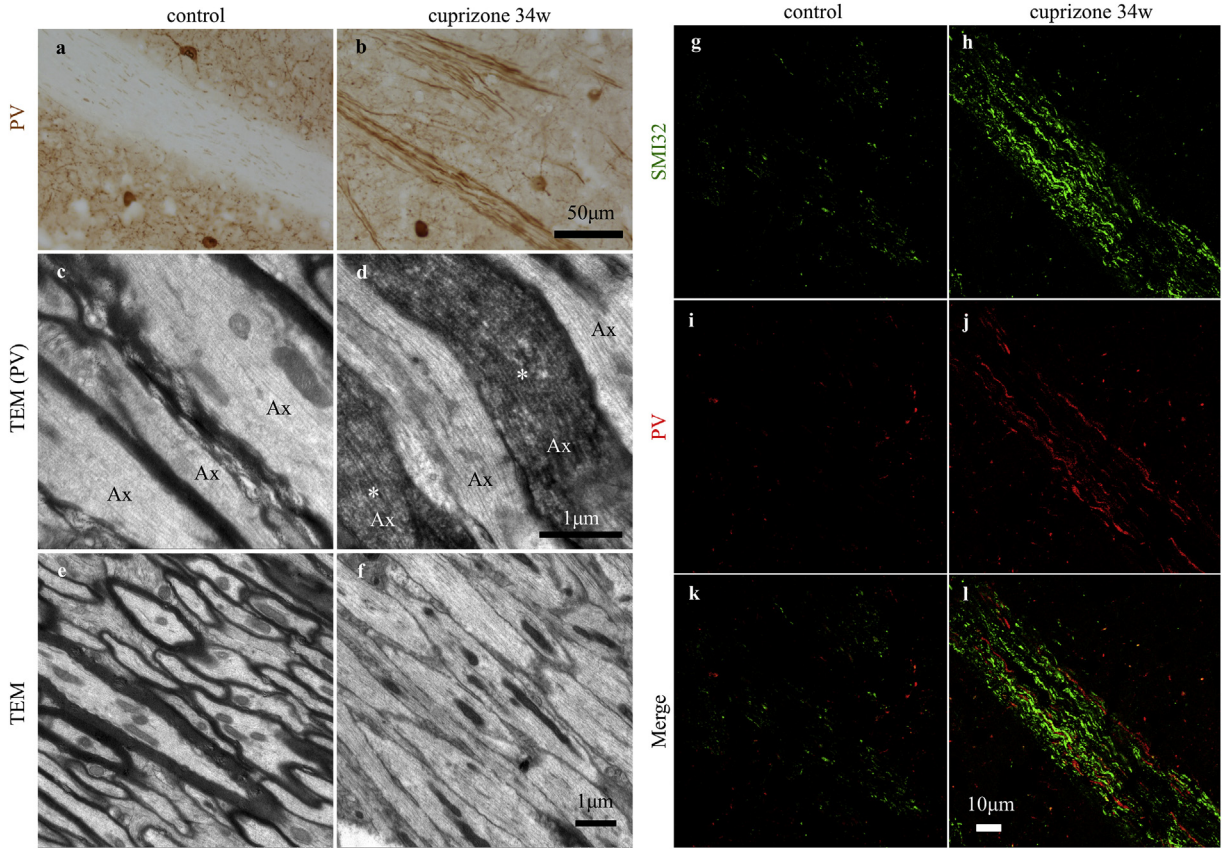

Fig. 5. PV increased cuprizone-induced demyelinated axons and PV positive axons tended to be protected from SMI32 positive axonal damage.
Representative images of PV immunohistochemistry in control and 34-week cuprizone administered mice are shown (a,b). In control mice, relatively small PV-positive neuronal somata in the grey matter and dot-like PV immunoreactivity in the white matter were observed (a). In mice with 34-week cuprizone administration, although the staining pattern of PV-positive neurons in the grey matter was not affected, PV-positive fiber-like immunoreactivity was increased in the white matter (b). Scale bar = 50 μm. Representative images of pre-embedding immunoelectron microscopy stained with PV in mice with control or 34-week cuprizone administered mice are shown (c,d). In control mice, many myelinated axons were observed and few axons were PV-positive (c). In mice with 34-week cuprizone administration, PV-positive demyelinated axons (asterisk) were increased (d). Scale bar = 1 μm. Representative images of transmission electron microscopy (TEM) in the striatum in mice with control or 34-week cuprizone diet are shown (e,f). In control mice, most axons were myelinated (e). In mice with 34-week cuprizone administration, although most axons were demyelinated, no degenerative axons were observed in the striatum (f). Ax: axon. Scale bar = 1 μm. Representative images of SMI32 and PV immunohistochemistry in the striatum in mice with control and 34-week cuprizone diet are shown (g–l). In control mice, little SMI32 and PV immunoreactivity was detected in the white matter in the striatum (g,i). However, in mice with 34-week cuprizone administration, increased immunoreactivity to SMI32 and PV was observed in the striatum (h,j). The merged view revealed that most SMI32 immunoreactivity did not co-localize with PV immunoreactivity (l). Scale bar = 10 μm.

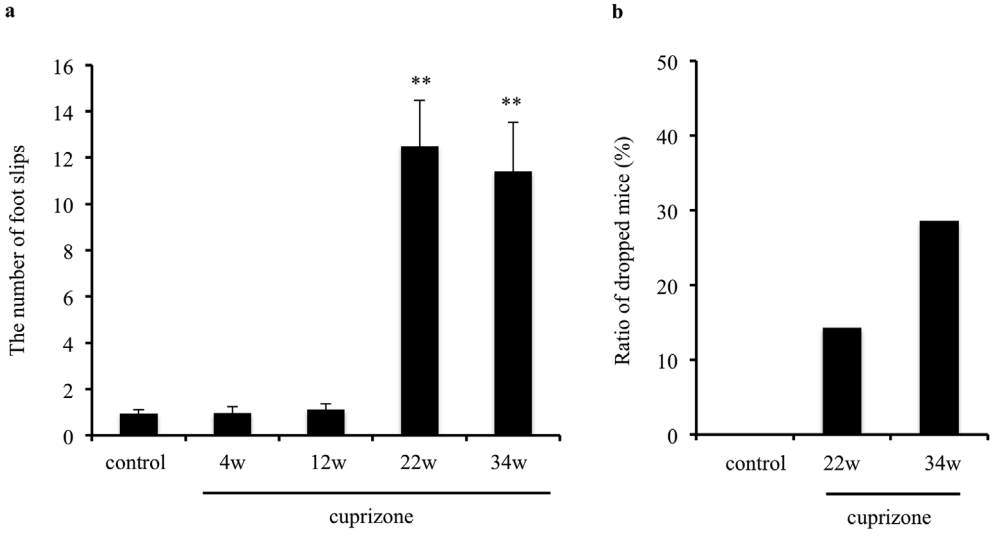

Fig. 6. Cuprizone induced motor coordination disorder as revealed by a balance beam test.
A balance beam test was performed on mice fed control or 4–34-week cuprizone diets. The number of foot slips and the ratio of falls in each group are shown in the graphs (a,b). In control mice, few foot slips were observed and 4 or 12-week cuprizone administration did not significantly increase foot slips (a). However, mice with 22 or 34-week cuprizone administration had significant increases in the number of foot slips compared to control mice (a). Control and 4 or 12-week cuprizone administered mice did not fall while crossing the beam (b). However, the ratio of mice that fell in mice with 22 or 34-week cuprizone administration increased (b). Data were obtained from 12 to 14 animals in each group (mean ± SEM; **P < 0.05, one-way ANOVA with Tukey-Kramer post hoc test for (a) and Fisher's exact test for (b).

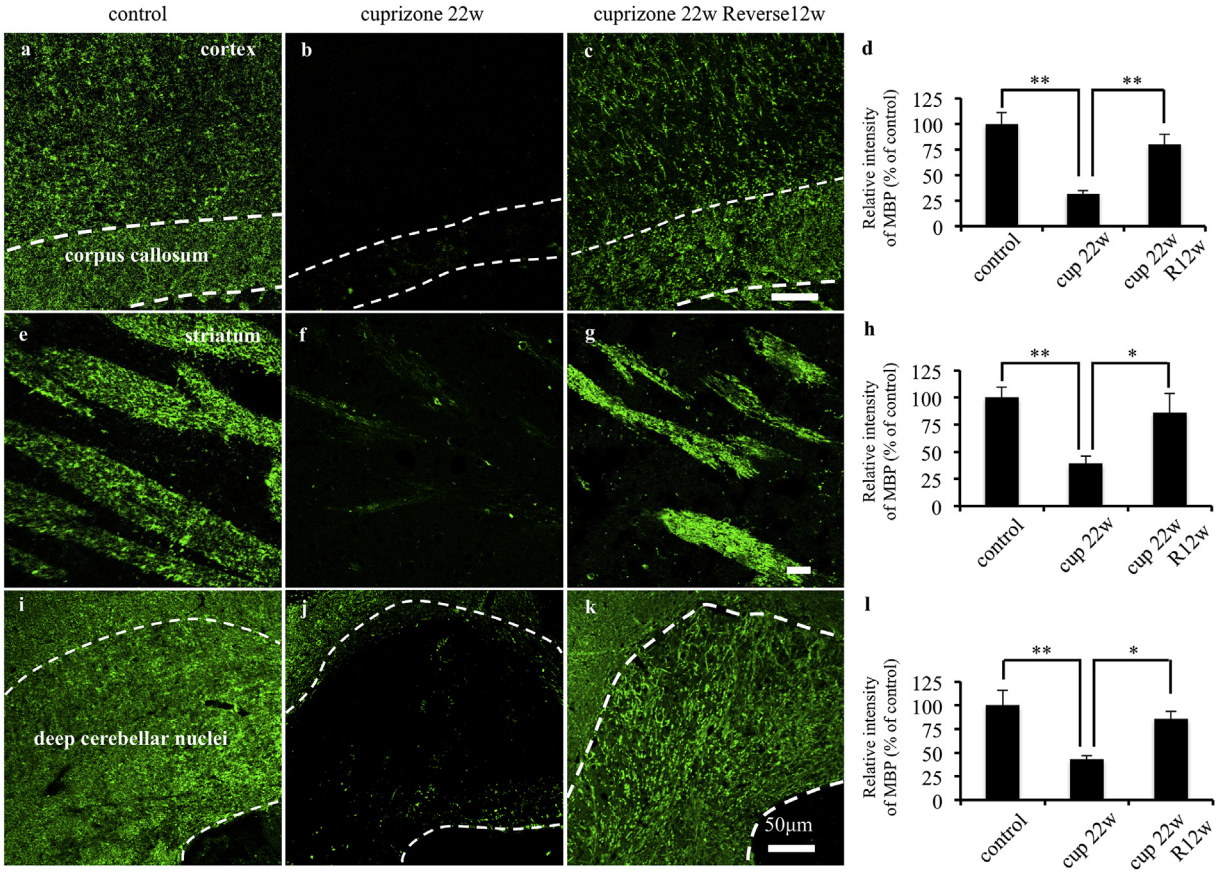

Fig. 7. Cuprizone-induced demyelination were reversed by 12-week withdrawal of cuprizone administration.
Representative images of MBP immunohistochemistry in the corpus callosum and cerebral cortex (a–c), striatum (e–g) and deep cerebellar cortex (i–k) in mice with control or 22-week cuprizone diet (cup22w) or 12-week recovery by normal diet following a 22-week cuprizone diet (cuprizone 22w Reverse 12w or cup22wR12w) are shown. In the cerebral cortex, striatum and deep cerebellar nuclei, while MBP immunoreactivity was evenly detected in control mice (a,e,i), in mice with 22-week cuprizone administration, MBP immunoreactivity in these regions decreased (b,f,j). However, in 12-week recovery following 22-week cuprizone administration, partial recovery of MBP immunoreactivity was detected in the cerebral cortex (c), striatum (g) and deep cerebellar nuclei (k). Scale bar = 50 μm. Semi-quantitative assessments of the intensity of MBP immunoreactivity in the cerebral cortex (d), striatum (h) and deep cerebellar nuclei (l) are shown in the graphs. Data were obtained from such images from 6 to 8 animals in each group (mean ± SEM; **P < 0.01, *P < 0.05, one-way ANOVA with Tukey-Kramer post hoc test).

86.05 ± 17.85%) (Fig. 7h) and deep cerebellar nuclei (control: 100.00 ± 15.92%, cuprizone 22w: 43.24 ± 3.27%, cuprizone 22w Reverse 12w: 85.58 ± 7.95%) (Fig. 7l). Furthermore, while the balance beam test showed that an increased number of mice with 22-week cuprizone administration fell (cuprizone 22w: 15.38%) as mentioned above, mice with 6 or 12-week recovery after cuprizone administration did not drop from the beam (Fig. 8a). Although mice with a 6-week recovery following 22-week cuprizone administration (cuprizone 22w Reverse 6w) did not significantly improve the number of foot slips compared to mice with 22-week cuprizone administration, another 6-

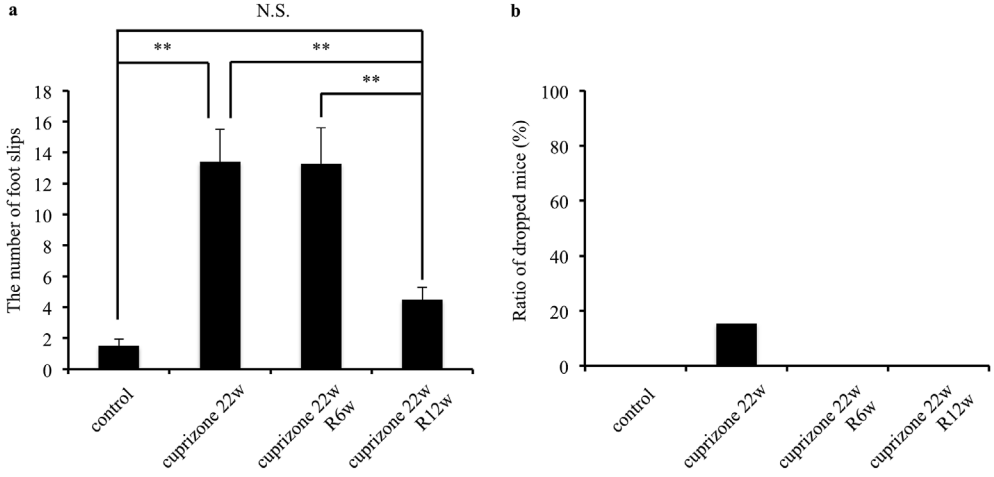

Fig. 8. Cuprizone-induced motor coordination disorder were reversed by 12-week withdrawal of cuprizone administration.
A balance beam test was performed on these mice. While few foot slips were observed in control mice, mice with 22-week cuprizone administration showed significantly more foot slips than those in control mice (a). Although 6-week recovery following 22-week cuprizone administration (cuprizone 22w Reverse 6w) did not significantly decrease the number of foot slips compared to that in mice with 22-week cuprizone diet, 12-week recovery (cuprizone 22w Reverse 12w) significantly decreased the number of foot slips compared to that in mice with 22-week cuprizone administration (a). Although some mice with 22-week cuprizone administration dropped from the beam, mice with 6 or 12-week recovery following cuprizone administration did not drop from the beam (b). Data were obtained from 12 to 13 animals in each group (mean ± SEM; **P < 0.05, one-way ANOVA with Tukey-Kramer post hoc test for (j), and Fisher's exact test for (k).

week recovery (cuprizone 22w Reverse 12w) significantly improved the number of foot slips compared to mice with 22-week cuprizone administration (control: 1.50 ± 0.43, cuprizone 22w: 13.41 ± 2.09, cuprizone 22w Reverse 6w: 13.29 ± 2.32, cuprizone 22w Reverse 12w: 4.50 ± 0.78) (Fig. 8b).

4. Discussion

In the present study, we demonstrated that there are regional differences in demyelination by cuprizone and in parvalbumin (PV) -positive neurons. Our results also suggest that continuous demyelination alone by long term cuprizone administration may not be enough to induce neuronal degeneration. Regional differences in sensitivity to cuprizone may explain why there are favored demyelination sites in multiple sclerosis (MS).

We showed that cuprizone administration induced severe demyelination in the cortex, corpus callosum, and deep cerebellar nuclei by 12 weeks, in agreement with previous reports (Kipp et al., 2017; Matsushima and Morell, 2001; Groebe et al., 2009; Gudi et al., 2014; Skripuletz et al., 2008). It had already been reported that in the striatum, partial demyelination was induced by 5-week cuprizone administration (Pott et al., 2009). However, it had been unknown whether longer cuprizone administration advanced demyelination in the striatum. We first revealed that cuprizone-induced demyelination advanced gradually up to 34 weeks in the striatum. In contrast, despite 34-week cuprizone administration, demyelination was not induced in the spinal cord or brainstem. These results imply that each region in the central nervous system (CNS) has differential sensitivity to demyelination.

In cuprizone-induced demyelination, damage to oligodendrocytes by cuprizone toxicity and microglial inflammation and phagocytosis are known to play key roles (Blakemore, 1972; Gudi et al., 2014; Matsushima and Morell, 2001; McMahon et al., 2001; Pasquini et al., 2007). Oligodendrocytes are heterogeneous cells present in many regions (Bechler et al., 2015; Marques et al., 2016). For example, oligodendrocytes in the striatum show a different gene expression pattern from those in the corpus callosum (Marques et al., 2016). Another study revealed that oligodendrocytes in the spinal cord form longer myelin sheaths than those in the cortex (Bechler et al., 2015). Therefore, different types of oligodendrocytes among regions may be responsible for the sensitivities to demyelination. Microglia also show regional phenotypes. For example, microglia are more phagocytic in the cerebellum and are more static in the striatum (Ayata et al., 2018). In our study, microglia had already increased both in the deep cerebellar nuclei and in the striatum by 4-week cuprizone administration. However, while it took 12 weeks to induce demyelination in the deep cerebellar nuclei, it took 34 weeks to induce demyelination in the striatum. These results may stem in part due to the different phenotypes of microglia between cerebellum and striatum. These glial differences among regions may be related to favored sites in MS. Further studies to elucidate glial function among regions are needed.

In the present study, cuprizone induced changes in PV-positive neurons. Intracellular localization of PV was changed in the cerebellum and striatum, but not in the cerebral cortex. PV is expressed in various types of neurons such as GABAergic interneurons in many regions including cerebral cortex and striatum (Jinno and Kosaka, 2004; Koós and Tepper, 1999; Lee et al., 2017; Tamamaki et al., 2010), cortical GABAergic neurons projecting to the striatum (Jinno and Kosaka, 2004; Tamamaki et al., 2010) and cortical glutamatergic neurons projecting to the striatum (Jinno and Kosaka, 2004). Reactions to cuprizone-induced demyelination may be different among the populations of PV-positive neurons. In the striatum, PV immunoreactivity appeared in demyelinated axons. Since PV is expressed in fast-firing neurons, PV-positive neurons are thought to be myelinated to satisfy high-energy demands (Celio, 1990; Stedehouder and Kushner, 2017). Therefore, PV-positive cells may be vulnerable to environmental disorders. Indeed, PV-positive neurons were impaired following demyelination in MS (Clements et al., 2008; Dutta et al., 2006). Two animal models of MS, experimental autoimmune encephalomyelitis (EAE) and the cuprizone model, are mainly used (Gudi et al., 2014; Kipp et al., 2017). These two models have some differences. EAE induces neuronal loss including PV-positive neurons leading severe paralysis (Aktas et al., 2005; Falco et al., 2014; Meyer et al., 2001; Vogt et al., 2009), and cuprizone-fed mice show no neuronal loss and mild motor-coordination dysfunction. It is possibly due to the difference of inflammatory reactions. EAE exhibits intense inflammation by microglia and lympohocytes (Aktas et al., 2005; Gudi et al., 2014; Vogt et al., 2009), however, cuprizone administration induces relatively mild inflammation mainly due to lack of lymphocyte infiltration (Bakker and Ludwin, 1987; Gudi et al., 2014). Although the cuprizone model is useful to study some aspects of neuronal pathological changes in neurons by demyelination and remyelination, this model holds some limitations.

PV is a calcium-binding protein that can protect cells from the toxic calcium overload in neuronal damage (Beers et al., 2001; Dekkers et al., 2004; Krieger et al., 1994; Verdaguer et al., 2015). It is probable that PV accumulated in axons during demyelination to protect from degeneration. However, to our knowledge, there is no report showing the role of PV in the axon. Further studies are needed.

In MS, long disease duration is a powerful risk factor for neurodegeneration following demyelination (Calabrese, 2013; Kutzelnigg et al., 2005; Larochelle et al., 2016; Vukusic and Confavreux, 2003). In the present study, we administered a 34-week cuprizone diet for sustained demyelination. However, unlike MS, no neuronal loss was observed. Although neurodegeneration in MS advances its clinical course without inflammatory attacks, diffuse inflammatory infiltrates and follicle-like lymphoid structures in the meninges are detected (Correale et al., 2017; Kipp et al., 2017; Larochelle et al., 2016; Magliozzi et al., 2007; Serafini et al., 2004). In contrast, no lymphocyte infiltration is observed in cuprizone-induced demyelination. Therefore, infiltration of lymphocytes may play a critical role in the induction of neuronal degeneration in addition to sustained demyelination.

It has been reported that withdrawal from a cuprizone diet reversed demyelination induced by up to 12-week cuprizone administration (Kipp et al., 2017; Matsushima and Morell, 2001; Gudi et al., 2014; Skripuletz et al., 2008). We showed that 22-week cuprizone-induced demyelination was also reveresed by following a 12-week withdrawal. In addition, cuprizone-induced motor-coordination dysfunction was also recovered along with remyelination. Therefore, mice with 22-week cuprizone administration may be useful models for examining the effects of drugs on histology and behavior.

5. Conclusions

In the present study, we demonstrated pathological changes caused by long term cuprizone administration in the CNS. Regional and neuronal vulnerability to demyelination were observed. However, cuprizone-induced sustained demyelination may not be sufficient to induce neurodegeneration, possibly due to the protective role of PV in Ca^{2+} buffering. Although neuronal degeneration was not observed, this model showed reversible demyelination and motor-coordination dysfunction. Therefore this model will be useful for investigating pathological and behavioral changes following demyelination in the CNS.

Conflicts of interest

Declarations of interest: none.

Acknowledgements

This work was supported by the Japan Society for the Promotion of Science (JSPS) KAKENHI Grant Number JP16K07023 (S.Y.), JP17K07087 (Y.B.), JP17K10052 (S.K.), and Grants from The Akiyama

Life Science Foundation (T.N.). We also thank Mr. Hazawa and Mr. Azuma for their technical supports and Dr. Saijo and Dr. Takakusaki for their advice. We thank Evan Hill, PhD, from Edanz Group (www.edanzediting.com/ac) for editing a draft of this manuscript.

Appendix A. Supplementary data

Supplementary data to this article can be found online at https://doi.org/10.1016/j.neuint.2019.03.018.

References

Aktas, O., Smorodchenko, A., Brocke, S., Infante-Duarte, C., Schulze, Topphoff U., Vogt, J., Prozorovski, T., Meier, S., Osmanova, V., Pohl, E., Bechmann, I., Nitsch, R., Zipp, F., 2005. Neuronal damage in autoimmune neuroinflammation mediated by the death ligand TRAIL. Neuron 46, 421–432.

Ayata, P., Badimon, A., Strasburger, H.J., Duff, M.K., Montgomery, S.E., Loh, Y.E., Ebert, A., Pimenova, A.A., Ramirez, B.R., Chan, A.T., Sullivan, J.M., Purushothaman, I., Scarpa, J.R., Goate, A.M., Busslinger, M., Shen, L., Losic, B., Schaefer, A., 2018. Epigenetic regulation of brain region-specific microglia clearance activity. Nat. Neurosci. 8, 1049–1060.

Baimbridge, K.G., Celio, M.R., Rogers, J.H., 1992. Calcium-binding proteins in the nervous system. Trends Neurosci. 15, 303–308.

Bakker, D.A., Ludwin, S.K., 1987. Blood-brain barrier permeability during Cuprizone-induced demyelination. Implications for the pathogenesis of immune-mediated demyelinating diseases. J. Neurol. Sci. 78, 125–137.

Bando, Y., Nomura, T., Bochimoto, H., Murakami, K., Tanaka, T., Watanabe, T., Yoshida, S., 2015. Abnormal morphology of myelin and axon pathology in murine models of multiple sclerosis. Neurochem. Int. 81, 16–27.

Bechler, M.E., Byrne, L., Ffrench-Constant, C., 2015. CNS myelin sheath lengths are an intrinsic property of oligodendrocytes. Curr. Biol. 25, 2411–2416.

Beers, D.R., Ho, B.K., Siklós, L., Alexianu, M.E., Mosier, D.R., Mohamed, A.H., Otsuka, Y., Kozovska, M.E., McAlhany, R.E., Smith, R.G., Appel, S.H., 2001. Parvalbumin overexpression alters immune-mediated increases in intracellular calcium, and delays disease onset in a transgenic model of familial amyotrophic lateral sclerosis. J. Neurochem. 79, 499–509.

Blakemore, W.F., 1972. Observations on oligodendrocyte degeneration, the resolution of status spongiosus and remyelination in cuprizone intoxication in mice. J. Neurocytol. 4, 413–426.

Calabrese, M., Romualdi, C., Poretto, V., Favaretto, A., Morra, A., Rinaldi, F., Perini, P., Gallo, P., 2013. The changing clinical course of multiple sclerosis: a matter of gray matter. Ann. Neurol. 74, 76–83.

Celio, M.R., 1990. Calbindin D-28k and parvalbumin in the rat nervous system. Neuroscience 35, 375–475.

Celio, M.R., Heizmann, C.W., 1981. Calcium-binding protein parvalbumin as a neuronal marker. Nature 293, 300–302.

Chen, Z.L., Momota, Y., Kato, K., Taniguchi, M., Inoue, N., Shiosaka, S., Yoshida, S., 1998. Expression of neuropsin mRNA in the mouse embryo and the pregnant uterus. J. Histochem. Cytochem. 46, 313–320.

Chort, A., Alves, S., Marinello, M., Dufresnois, B., Dornbierer, J.G., Tesson, C., Latouche, M., Baker, D.P., Barkats, M., El Hachimi, K.H., Ruberg, M., Janer, A., Stevanin, G., Brice, A., Sittler, A., 2013. Interferon β induces clearance of mutant ataxin 7 and improves locomotion in SCA7 knock-in mice. Brain 136, 1732–1745.

Clements, R.J., McDonough, J., Freeman, E.J., 2008. Distribution of parvalbumin and calretinin immunoreactive interneurons in motor cortex from multiple sclerosis post-mortem tissue. Exp. Brain Res. 187, 459–465.

Correale, J., Gaitán, M.I., Ysrraelit, M.C., Fiol, M.P., 2017. Progressive multiple sclerosis: from pathogenic mechanisms to treatment. Brain 140, 527–546.

Dekkers, J., Bayley, P., Dick, J.R., Schwaller, B., Berchtold, M.W., Greensmith, L., 2004. Over-expression of parvalbumin in transgenic mice rescues motoneurons from injury-induced cell death. Neuroscience 123, 459–466.

Dutta, R., McDonough, J., Yin, X., Peterson, J., Chang, A., Torres, T., Gudz, T., Macklin, W.B., Lewis, D.A., Fox, R.J., Rudick, R., Mirnics, K., Trapp, B.D., 2006. Mitochondrial dysfunction as a cause of axonal degeneration in multiple sclerosis patients. Ann. Neurol. 59, 478–489.

Falco, A., Pennucci, R., Brambilla, E., de Curtis, I., 2014. Reduction in parvalbumin-positive interneurons and inhibitory input in the cortex of mice with experimental autoimmune encephalomyelitis. Exp. Brain Res. 232, 2439–2449.

Groebe, A., Clarner, T., Baumgartner, W., Dang, J., Beyer, C., Kipp, M., 2009. Cuprizone treatment induces distinct demyelination, astrocytosis, and microglia cell invasion or proliferation in the mouse cerebellum. Cerebellum 8, 163–174.

Gudi, V., Gingele, S., Skripuletz, T., Stangel, M., 2014. Glial response during cuprizone-induced de- and remyelination in the CNS: lessons learned. Front. Cell. Neurosci. 8, 1–24.

Jinno, S., Kosaka, T., 2004. Parvalbumin is expressed in glutamatergic and GABAergic corticostriatal pathway in mice. J. Comp. Neurol. 477, 188–201.

Kipp, M., Nyamoya, S., Hochstrasser, T., Amor, S., 2017. Multiple sclerosis animal models: a clinical and histopathological perspective. Brain Pathol. 27, 123–137.

Koós, T., Tepper, J.M., 1999. Inhibitory control of neostriatal projection neurons by GABAergic interneurons. Nat. Neurosci. 2, 467–472.

Krieger, C., Jones, K., Kim, S.U., Eisen, A.A., 1994. The role of intracellular free calcium in motor neuron disease. J. Neurol. Sci. 124 (Suppl. l), 27–32.

Kutzelnigg, A., Lucchinetti, C.F., Stadelmann, C., Brück, W., Rauschka, H., Bergmann, M., Schmidbauer, M., Parisi, J.E., Lassmann, H., 2005. Cortical demyelination and diffuse white matter injury in multiple sclerosis. Brain 128, 2705–2712.

Larochelle, C., Uphaus, T., Prat, A., Zipp, F., 2016. Secondary progression in multiple sclerosis: neuronal exhaustion or distinct pathology? Trends Neurosci. 39, 325–339.

Lee, K., Holley, S.M., Shobe, J.L., Chong, N.C., Cepeda, C., Levine, M.S., Masmanidis, S.C., 2017. Parvalbumin interneurons modulate striatal output and enhance performance during associative learning. Neuron 93, 1451–1463.

Luong, T.N., Carlisle, H.J., Southwell, A., Patterson, P.H., 2011. Assessment of motor balance and coordination in mice using the balance beam. JoVE 49, 2376.

Magliozzi, R., Howell, O., Vora, A., Serafini, B., Nicholas, R., Puopolo, M., Reynolds, R., Aloisi, F., 2007. Meningeal B-cell follicles in secondary progressive multiple sclerosis associate with early onset of disease and severe cortical pathology. Brain 130, 1089–1104.

Marques, S., Zeisel, A., Codeluppi, S., van Bruggen, D., Mendanha Falcão, A., Xiao, L., Li, H., Häring, M., Hochgerner, H., Romanov, R.A., Gyllborg, D., Muñoz Manchado, A., La Manno, G., Lönnerberg, P., Floriddia, E.M., Rezayee, F., Ernfors, P., Arenas, E., Hjerling-Leffler, J., Harkany, T., Richardson, W.D., Linnarsson, S., Castelo-Branco, G., 2016. Oligodendrocyte heterogeneity in the mouse juvenile and adult central nervous system. Science 352, 1326–1329.

Matsushima, G.K., Morell, P., 2001. The neurotoxicant, cuprizone, as a model to study demyelination and remyelination in the central nervous system. Brain Pathol. 11, 107–116.

McMahon, E.J., Cook, D.N., Suzuki, K.M., 2001. Absence of macrophage-inflammatory protein-1 alpha delays central nervous system demyelination in the presence of an intact blood-brain barrier. J. Immunol. 167, 2964–2971.

Meyer, R., Weissert, R., Diem, R., Storch, M.K., de Graaf, K.L., Kramer, B., Bahr, M., 2001. Acute neuronal apoptosis in a rat model of multiple sclerosis. J. Neurosci. 21, 6214–6220.

Nomura, T., Bando, Y., Bochimoto, H., Koga, D., Watanabe, T., Yoshida, S., 2013. Three-dimensional ultra-structures of myelin and the axons in the spinal cord: application of SEM with the osmium maceration method to the central nervous system in two mouse models. Neurosci. Res. 75, 190–197.

Nomura, T., Bando, Y., You, H., Tanaka, T., Yoshida, S., 2017. Yokukansan reduces cuprizone-induced demyelination in the corpus callosum through anti-inflammatory effects on microglia. Neurochem. Res. 42, 3525–3536.

Pasquini, L.A., Calatayud, C.A., Bertone, Uña A.L., Millet, V., Pasquini, J.M., Soto, E.F., 2007. The neurotoxic effect of cuprizone on oligodendrocytes depends on the presence of pro-inflammatory cytokines secreted by microglia. Neurochem. Res. 32, 279–292.

Pott, F., Gingele, S., Clarner, T., Dang, J., Baumgartner, W., Beyer, C., Kipp, M., 2009. Cuprizone effect on myelination, astrogliosis and microglia attraction in the mouse basal ganglia. Brain Res. 1305, 137–149.

Reich, D.S., Lucchinetti, C.F., Calabresi, P.A., 2018. Multiple sclerosis. N. Engl. J. Med. 378, 169–180.

Serafini, B., Rosicarelli, B., Magliozzi, R., Stigliano, E., Aloisi, F., 2004. Detection of ectopic B-cell follicles with germinal centers in the meninges of patients with secondary progressive multiple sclerosis. Brain Pathol. 14, 164–174.

Skripuletz, T., Lindner, M., Kotsiari, A., Garde, N., Fokuhl, J., Linsmeier, F., Trebst, C., Stangel, M., 2008. Cortical demyelination is prominent in the murine cuprizone model and is strain-dependent. Am. J. Pathol. 172, 1053–1061.

Stedehouder, J., Kushner, S.A., 2017. Myelination of parvalbumin interneurons: a parsimonious locus of pathophysiological convergence in schizophrenia. Mol. Psychiatr. 1, 4–12.

Tamamaki, N., Tomioka, R., 2010. Long-range GABAergic connections distributed throughout the neocortex and their possible function. Front. Neurosci. 4, 202.

Tanaka, T., Murakami, K., Bando, Y., Yoshida, S., 2013. Minocycline reduces remyelination by suppressing ciliary neurotrophic factor expression after cuprizone-induced demyelination. J. Neurochem. 127, 259–270.

Terayama, R., Bando, Y., Takahashi, T., Yoshida, S., 2004. Differential expression of neuropsin and protease M/neurosin in oligodendrocytes after injury to the spinal cord. Glia 48, 91–101.

Verdaguer, E., Brox, S., Petrov, D., Olloquequi, J., Romero, R., de Lemos, M.L., Camins, A., Auladell, C., 2015. Vulnerability of calbindin, calretinin and parvalbumin in a transgenic/knock-in APPswe/PS1dE9 mouse model of Alzheimer disease together with disruption of hippocampal neurogenesis. Exp. Gerontol. 69, 176–188.

Vogt, J., Paul, F., Aktas, O., Müller-Wielsch, K., Dörr, J., Dörr, S., Bharathi, B.S., Glumm, R., Schmitz, C., Steinbusch, H., Raine, C.S., Tsokos, M., Nitsch, R., Zipp, F., 2009. Lower motor neuron loss in multiple sclerosis and experimental autoimmune encephalomyelitis. Ann. Neurol. 66, 310–322.

Vukusic, S., Confavreux, C., 2003. Prognostic factors for progression of disability in the secondary progressive phase of multiple sclerosis. J. Neurol. Sci. 206, 135–137.

Yoshida, S., Lin, L.P., Chen, Z.L., Momota, Y., Kato, K., Tanaka, T., Wanaka, A., Shiosaka, S., 1994. Basal magnocellular and pontine cholinergic neurons coexpress FGF receptor mRNA. Neurosci. Res. 20, 35–42.